Short- and long-range-order effects on the electronic properties of III-V semiconductor alloys

Kurt A. Mäder and Alex Zunger
National Renewable Energy Laboratory, Golden, Colorado 80401
(Received 6 September 1994)

First-principles and empirical pseudopotentials are used to study the effects of short-range and long-range atomic order on the electronic properties of III-V semiconductor alloys. The alloy structure with a given degree of long- or short-range order is modeled by two types of supercells: (a) Small (16–32 atom) supercells are constructed in the fashion of the special quasirandom structures (SQS) used previously to simulate random alloys [A. Zunger *et al.*, Phys. Rev. Lett. **65**, 353 (1990)]. Their electronic structure is treated via first-principles pseudopotential methods. (b) Large ($\sim$1000 atom) supercells are found by a simulated-annealing technique which optimizes the atomic configuration until a given degree of short-range order is reproduced. The electronic structure is then determined using the empirical pseudopotential method. Statistical tests prove that the small cell SQS mimic the much larger supercells and thus provide an efficient means of studying the electronic band structure of disordered alloys in a non-mean-field approach. For the direct band gaps of ideally random $Al_{1-x}Ga_xAs$, $Ga_{1-x}In_xP$, and $Al_{1-x}In_xAs$ alloys, we find optical bowing parameters $b=0.48$, 0.46, and 0.52 eV, respectively. In the presence of short-range order in the form of cation clustering, we find the following: (i) Clustering elongates the Ga-P bond and shortens the In-P bond in $Ga_{0.5}In_{0.5}P$ and (ii) the optical bowing of the direct band gap is greatly enhanced. This leads to an indirect-gap to direct-gap crossover in $Al_{0.5}Ga_{0.5}As$ with sufficient clustering. (iii) The band-gap reduction is accompanied by a localization of band-edge wave functions on certain types of clusters. The clusters act as "isoelectronic impurities" which localize states if their concentration (i.e., the degree of short-range order) is large enough. Electrons at the conduction-band minimum localize on the cations with lower *s*-orbital energies. The band-gap reduction and wave-function localization of alloys with short-range order is compared to the effects of long-range order, where the gap reduction is due to level repulsion between zone-folding conduction states. Numerical results are given for CuPt-type long-range order of $AlGaAs_2$, $GaInP_2$, and $AlInAs_2$. For complete ordering, the band-gap reduction relative to the random alloys are 0.36, 0.49, and 0.16 eV, respectively.

I. INTRODUCTION

Pseudobinary $A_{1-x}B_xC$ semiconductor alloys exhibit deviations from perfect random arrangements of the A and B atoms on their fcc sublattice.[1] These deviations take the form of long-range order (LRO), short-range order (SRO), or both. LRO in III-V alloys appears most frequently in the CuPt structure [an $(AC)_1(BC)_1$ monolayer superlattice along $\langle 111 \rangle$] and is accompanied by a reduction in the band gap relative to the disordered phase.[2–4] This gap reduction reflects zone folding and level repulsion[5] and depends quadratically[6] on the degree η of LRO.

In contrast to LRO, studies of the effects of SRO on alloy band gaps are scarce. The degree of SRO is generally quantified by the Warren-Cowley[7] parameter

$$\alpha_j = 1 - \frac{P_B(j)}{x_B} , \tag{1}$$

where $P_B(j)$ is the probability of finding a B atom on the jth nearest-neighbor shell about A as an origin, and x_B is the concentration of B atoms. In the perfect random alloy $P_B(j)=x_B$ and thus $\alpha_j=0$ for all atomic shells. Preferred association of *like atoms* ("clustering") means $\alpha>0$, whereas association of *unlike atoms* ("anticlustering") is manifested by $\alpha<0$. Thermodynamically, clustering and anticlustering tendencies are decided by the energy change when the site occupancy is altered from random to phase-separated or ordered structures, respectively. In semiconductors, this depends largely on strain. Theory[8,9] shows that in such alloys much of the energy is decided by elastic effects associated with packing size-mismatched constituents onto a given lattice. There are two extreme possible elastic states of the phase-separated system (AC-rich and BC-rich domains): either these domains adopt the average lattice constant $\bar{a}(x)$ of the homogeneous alloy from which they precipitated ("coherent phase separation"), or each component (AC and BC) relaxes, adopting its own free-space equilibrium lattice constant a_{AC} and a_{BC}, respectively ("incoherent phase separation"). Calculations showed that if coherence is maintained, then one expects anticlustering[9] [because the energy of $AC+BC$ strained to $\bar{a}(x)$ is higher than the energy of locally ordered structures at the same $\bar{a}(x)$]. On the other hand, if the constituents are relaxed (incoherent phase separation), their energy is lowered and the ground state is phase separation, so clustering is expected.

Direct measurements of SRO in tetrahedral semiconductor alloys were carried out by diffuse x-ray scattering,[10–16] transmission electron microscopy,[17,18] and scan-

ning tunneling microscopy.[19,20] Indirect evidence for SRO comes from nuclear magnetic resonance,[21–23] Raman scattering,[24–27] infrared reflectivity,[28–30] photoluminescence,[31–34] and photoreflectance.[35] Some experiments on semiconductor alloys[11,15,18–20,28–30,35] report clustering-type SRO ($\alpha>0$), others[14,22,23] report anticlustering ($\alpha<0$), and some[12,13,32] suggest near-perfect randomness ($\alpha\approx 0$). Despite these extensive studies, little is known about the effects of SRO on band gaps.[36–38] Because some degree of SRO or LRO is always present in the technologically important III-V semiconductor alloys, a good understanding of their effects on the electronic and optical properties is important. Controlled use of these structural "degrees of freedom" may provide additional tools for band-gap engineering. In this paper we report results of pseudopotential calculations on the band gaps of perfectly random ($\alpha=0$) as well as clustered ($\alpha>0$) models of $Al_{0.5}Ga_{0.5}As$, $Ga_{0.5}In_{0.5}P$, and $Al_{0.5}In_{0.5}As$ alloys. The results are compared with the effects of LRO. We use structures whose sites are occupied by A, B, and C atoms so as to create given degrees of short- or long-range order in the AB sublattice. This requires unit cells with 16–1024 atoms. Atomic positions are then relaxed to minimize the total energy. We find that local clustering can (i) reduce the band gap of III-V alloys to a similar extent as LRO does, (ii) transform the indirect-gap material $Al_{0.5}Ga_{0.5}As$ into a direct-gap one, and (iii) localize the band-edge wave functions preferentially on a particular type of cluster, even though an *isolated* nearest-neighbor cluster does not produce a bound state. We explain the wave-function localization and band-gap reduction in terms of two complementary mechanisms: an "impurity" picture and a "quantum-well" picture. We discuss the chemical trends in the cation sequence Al→Ga→In. A brief preliminary account was given by us in Ref. 39.

II. METHODOLOGY

In this section we describe the main ideas behind the computational methods used in this work. Details are given in the Appendix, or published in archive form.

To calculate the electronic energy-level spectrum and wave functions of a disordered solid, we need (i) a structural model, which accurately simulates the chemical and positional disorder in the system, (ii) a Hamiltonian, which describes the electron dynamics in such structures, and (iii) a method for solving the Schrödinger equation. Our approach to (i), (ii), and (iii) will be described in Secs. II A, II B, and II C, respectively. The structural and electronic models are combined in Sec. II D to provide the necessary tools for a spectral analysis of the electronic structure of disordered alloys.

A. Structural models for alloys with short- or long-range order

In a binary substitutional alloy with N atomic sites there are 2^N distinct ways (configurations σ) to occupy sites by A and B atoms. We are interested in calculating *configurational averages* of lattice properties $P(\sigma)$, e.g., band gaps, bond lengths, and formation energies. Denoting the configurational average with angular brackets, we have

$$\langle P\rangle=\sum_{\sigma}P(\sigma)\rho(\sigma)\ , \tag{2}$$

where ρ is the normalized configurational density matrix.[40] For example, in a perfectly random alloy ($\alpha=\eta=0$) at composition $x=0.5$, all configurations have equal probability, thus $\rho(\sigma)=2^{-N}\ \forall\sigma$. For disordered systems with SRO or LRO, however, $\rho(\sigma)$ is no longer a constant.

There are several approaches to estimate $\langle P\rangle$. The first is to calculate $P(\sigma)$ directly for a sufficiently large number of configurations, and then compute the average $\langle P\rangle$ from Eq. (2), with a given (random or nonrandom) density matrix ρ. Equivalently, one can construct *one* very large sample, and calculate $P(\sigma)$ for this particular configuration. Approximations to this approach in the context of tight-binding Hamiltonians have been offered for random $Al_{0.5}Ga_{0.5}As$ by Hass, Davis, and Zunger[41] and for random $ZnSe_{1-x}Te_x$ by Li and Pötz,[42] while Silverman *et al.*[43] used this approach for $Ga_{0.5}In_{0.5}P$ in the context of Monte Carlo simulations.

A second approach consists of choosing a suitable orthonormal basis in configuration space (the inner product being a sum over all 2^N configurations), and expanding P and ρ in terms of this basis. This is the concept behind the Ising-like "cluster expansion,"[44,45] where the basis functions are products Π_f over pseudospin variables $\hat{S}_i$ in "figures" f (single site, pair, triplet, etc.) of atomic sites. Then, for any configuration σ one expands $P(\sigma)$ in a hierarchy of figures:

$$P(\sigma)=\sum_{f}p_f D_f\overline{\Pi}_f(\sigma)\ , \tag{3}$$

where p_f is the contribution of figure f to the property P, $\overline{\Pi}_f(\sigma)$ is a lattice average of the spin products over symmetry-equivalent figures, and D_f is a degeneracy factor. The distinctive feature of this approach is that the configurational average of $P(\sigma)$ is written in terms of the average of the $\overline{\Pi}_f(\sigma)$'s, rather than averages over configurations, i.e.,

$$\langle P\rangle=\sum_{f}p_f D_f\langle\overline{\Pi}_f\rangle\ , \tag{4}$$

where $\langle\overline{\Pi}_f\rangle=\sum_\sigma\overline{\Pi}(\sigma)\rho(\sigma)$ are "multisite correlation functions." The contribution p_f of figure f can be calculated[45] from the property $P(\sigma)$ of some ordered configurations $\{\sigma\}$. The success of a cluster expansion[45] relies on the fact that for many physical quantities $P(\sigma)$ the parameters p_f fall off rapidly with increasing separation between the sites, and with increasing number of vertices in figure f. Therefore only a few p_f's are needed in Eq. (4).

A third approach to finding configurational averages $\langle P\rangle$ is to identify the leading terms of Eq. (4) and then construct a *single special configuration* σ_s whose $\overline{\Pi}_f(\sigma_s)$ match the given configurational *averages* $\langle\overline{\Pi}_f\rangle$ for these "important" figures.[46] One then calculates *directly* $P(\sigma_s)$

for the single, special configuration σ_s *without* using any cluster expansion. $\langle P \rangle$ is thus approximated by $P(\sigma_s)$. For the random binary alloy $A_{1-x}B_x$ the correlation functions $\langle \overline{\Pi}_f \rangle$ are known trivially, i.e., $\langle \overline{\Pi}_f \rangle = (2x-1)^{k_f}$, where k_f is the number of vertices in figure f. A special configuration which matches these correlation functions up to a maximum figure is called[46] a "special quasirandom structure" (SQS). Surprisingly, one can find periodic SQS's with only ~ 16 sites that have zero deviations from the "ideal" correlation functions for pair figures up to the seventh atomic shell. Direct calculation[41] of their band structure reproduces remarkably well the results obtained with huge supercells. This approach has been applied to various properties of semiconductor[38,46,47] and transition-metal[48] alloys.

While previous applications of SQS[38,46–48] concentrated on perfectly random phases, *any* state of order can be described by the set of lattice-averaged spin products $\{\overline{\Pi}_f(\sigma)\}$. For example, the SRO parameters α_j of Eq. (1) are related to the pair-correlation functions through

$$\alpha_j = \frac{\langle \overline{\Pi}_{(2,j)} \rangle - q^2}{1-q^2} , \tag{5}$$

where $f=(2,j)$ denotes the jth nearest-neighbor pair figure, and $q=2x-1$. The long-range-order parameter η, on the other hand, measures the relative *concentration* of foreign atoms on each sublattice, and if we assume absence of correlations among atoms on the *same* sublattice we obtain for the pair-correlation functions[6]

$$\langle \overline{\Pi}_{(2,j)}(\eta) \rangle = q^2 + \eta^2 [\overline{\Pi}_{(2,j)}(\sigma) - q_\sigma^2] . \tag{6}$$

Here, $q_\sigma = 2X_\sigma - 1$, where X_σ is the composition of the fully ordered structure σ. We can thus characterize SRO [Eq. (5)] or LRO [Eq. (6)] by the correlation functions and construct special structures that mimic them. Thus for either SRO [Eq. (5)] or LRO [Eq. (6)] we can search for "special" configurations σ_s which minimize a "cost function" Q_s defined as

$$Q_s(\sigma) = \sum_f w_f D_f [\langle \overline{\Pi}_f \rangle - \overline{\Pi}_f(\sigma)]^2 , \tag{7}$$

where the weights w_f are chosen to reflect the estimated magnitude of the interaction parameters p_f, and are zero beyond a specified maximum figure. Anticipating applications of band-structure techniques to the SQS's, we further restrict the search to *periodic structures*. We will denote these structures with N sites per unit cell as SQS-N (even if they are not "quasirandom," but exhibit some degree of SRO or LRO). For $N \leq 16$ an *explicit* search among all configurations is feasible.[49] For larger N, we use a simulated-annealing scheme[50] to find SQS's which minimize Q_s. We start by choosing a unit cell with N atomic sites, and randomly assign pseudospins $\hat{S}_j = \pm 1$ to each site. We then perform spin flips using the Metropolis algorithm[51] with Q_s of Eq. (7) as the "energy," thus accepting or rejecting the new configuration. Annealing to low "temperature" will then freeze out structures which are good SQS's.

Our purpose here is to identify the primary fingerprints of SRO on the band gap and wave functions of otherwise random alloys. Thus, rather than use realistic but complex SRO parameters found in full thermodynamic phase diagram simulations,[9,43] we concentrate on the electronic consequences of the *leading forms of SRO*. To this end we have constructed SQS's for $\alpha_1 = +K$ and $\alpha_1 = -K$ (clustering and anticlustering of the first shell, respectively), setting $\alpha_j = 0$, for all shells $j > 1$. We use $K = \frac{1}{6}$, which gives a substantial effect. The results are compared with SQS for $\alpha = 0$, representing the random alloy. For LRO, we use SQS's for CuPt-type ordering with $\eta = \frac{1}{2}$, $\eta = 1/\sqrt{2}$, and the fully ordered CuPt structure with $\eta = 1$. These SQS's have $N = 8$,16, 108, and 512 fcc sites per unit cell, and those for LRO have $N = 8$ and 16. The unit cells parameters and atomic positions of all of these SQS's are available electronically.[52] Their quality is demonstrated in the Appendix. Including in Eq. (7) seven pair and the nearest-neighbor triplet and quadruplet figures, we find a *random* SQS-16 with $Q_s = 0$, i.e., all included correlations reproduce exactly the infinite random alloy. With the simulated-annealing technique (using a fixed supercell geometry), $N \gtrsim 500$ lattice sites are typically needed to achieve such a good quality, i.e., $Q_s = 0$. For the $\alpha = 0$ SQS-8 the first small error in a pair-correlation function occurs at the third shell ($\overline{\Pi}_{(2,3)} = \frac{1}{24}$). For the $\alpha = \frac{1}{6}$ SQS-8 the first error occurs at the fifth shell ($\overline{\Pi}_{(2,5)} = -\frac{1}{6}$). Another statistical test is the comparison of the distribution of $A_{4-n}B_n$, $n = 0, \ldots, 4$, tetrahedral clusters in the SQS with the exact random values. The cluster distribution depends linearly on the composition and the nearest-neighbor figures (pair, triplet, and quadruplet), and obeys a Bernoulli distribution in the case of the random alloy. We find that this distribution is exactly matched by the $\alpha = 0$ SQS-8 and SQS-16 (see the Appendix). The overall statistical quality of the SQS-N used here is excellent, given that the smallest SQS has only eight fcc sites.

So far we have discussed the *topology* of alloy structures. To determine the *geometry* we allow atoms to relax to their (local) minimum energy position without swapping sites. We perform this relaxation using Keating's valence force field (VFF) model.[53,54] For the SQS-8 we confirm the validity of the VFF model by performing a first-principles local-density-approximation (LDA) calculation, and relaxing the structural degrees of freedom using quantum-mechanical forces.

The VFF model provides a further test for the accuracy of the SQS approach as it affords comparison of the elastic energies of the SQS's with those of very large supercells. Table I gives results of our VFF calculations on $Ga_{0.5}In_{0.5}P$ using SQS-8 and SQS-512. The formation energies ΔH_{ur} of the *unrelaxed* structures agree perfectly, while those of the relaxed lattice (ΔH_r) are within 10%. Bond lengths calculated with small and large SQS's agree within 0.1%. Figure 1 shows the VFF elastic energy of $Ga_{0.5}In_{0.5}P$ as a function of the CuPt-type LRO parameter η squared. We compare the well-converged results from 1024-atom supercells (SQS-512) with those from 16-atom supercells (SQS-8), finding the SQS-8 results to be good approximations to the converged values. Thus

TABLE I. VFF results (Ref. 53) for relaxed (subscript r) and unrelaxed (subscript ur) $Ga_{0.5}In_{0.5}P$ SQS. ΔH and V are the formation energy and volume per $GaInP_2$ formula unit, respectively. The equilibrium bond lengths are $R^0_{Ga\text{-}P}=2.360$ Å, $R^0_{In\text{-}P}=2.541$ Å.

	$\alpha=-\frac{1}{6}$		$\alpha=0$		$\alpha=+\frac{1}{6}$	
Quantity	SQS-8	SQS-512	SQS-8	SQS-512	SQS-8	SQS-512
ΔH_{ur} (meV)	324.1	324.1	324.9	324.9	325.7	325.7
ΔH_r (meV)	80.6	81.1	86.0	91.0	111.5	100.2
V_{ur} (a.u.)	599.1	599.1	599.1	599.1	599.1	599.1
V_r (a.u.)	595.2	595.2	595.2	595.0	594.7	594.9
R(Ga-P)	2.377±0.011	2.377±0.012	2.379±0.009	2.380±0.014	2.386±0.021	2.383±0.015
R(In-P)	2.518±0.007	2.518±0.009	2.516±0.011	2.515±0.011	2.509±0.015	2.512±0.012

the small SQS gives an adequate approximation. Relaxation of the SQS's reduces the elastic energy by about 70% with respect to the unrelaxed structures. This involves relatively large relaxation of the bond lengths towards their respective zinc-blende equilibrium values. This is also illustrated in Table I, where we give the nearest-neighbor (cation-anion) distances as a function of the SRO parameter α. Relative to the random alloy, the cation-anion bond lengths relax slightly more in the presence of anticlustering SRO and less in the presence of clustering SRO. The short Ga-P bond elongates a bit due to clustering while the long In-P bond shortens a bit due to clustering. The calculated Ga-P and In-P bond lengths at $\alpha=0$ agree very well with experiment,[55] which gives R(Ga-P)=2.379±0.010 Å and R(In-P)=2.519±0.010 Å. Our calculated values are 2.380±0.014 and 2.515±0.011 Å for the Ga-P and In-P bonds, respectively (Table I). We note that agreement between theory and experiment is better than the experimental uncertainty. Furthermore, our SQS-512 results indicate that the standard deviation of the bond-length distribution is of the same order as the experimental uncertainty (~0.01 Å).

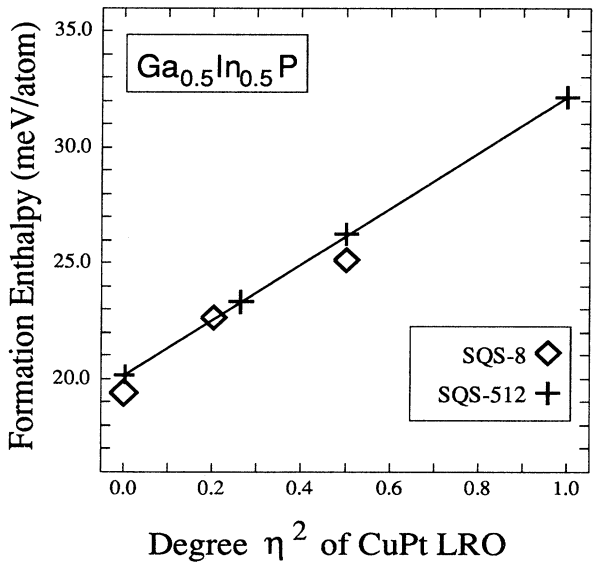

FIG. 1. VFF formation energy of $Ga_{0.5}In_{0.5}P$ with CuPt-type LRO as a function of the LRO parameter η squared. Symbols are SQS-N calculations; the solid line is a quadratic interpolation between the SQS-512 result for $\eta=0$ and the result for perfect CuPt ordering ($\eta=1$).

The structural model used here to represent random alloys or alloys with SRO differs from the structural models underlying the virtual-crystal approximation (VCA) or the single-site coherent potential approximation (s-CPA). The VCA assumes all atoms on the mixed sublattice to be identical, and the s-CPA assumes A and B atoms to each have their respective mean-field-like environment. The s-CPA thus neglects differences in the local environments of the individual atoms, which would result in different charge transfers (and thus a change in the Madelung energy[56]) and bond lengths.[48] In contrast, the N sites in a SQS-N are in general not equivalent.[57] An empirical tight-binding implementation of the s-CPA has been applied to pseudobinary III-V alloys to study electronic properties associated with random disorder by Chen and Sher.[58]

B. Empirical pseudopotentials

The periodic structures with special site occupations that represent a given degree of SRO or LRO are now used to model the electronic structure of disordered alloys. Although we extensively will use SQS's with a "small" number of atoms ($N=8$ or 16 fcc sites) for which LDA calculations are practical, it is also desirable to use large SQS's so that extremely well-converged SQS results can be established. To this end the electronic structure of large SQS's of $Al_{0.5}Ga_{0.5}As$ was calculated using carefully fitted empirical, atomic pseudopotentials in a plane-wave basis.[59]

To achieve an accurate description of the electronic structure of a large variety of atomic configurations, we fitted the atomic pseudopotentials to (i) the band structures of the binaries, (ii) the valence-band offset between the binaries, (iii) the correct "scattering strength" in various substitutional configurations as reflected by LDA-calculated level splittings in short-period superlattices, (iv) the effective masses, and (v) the deformation potentials. Reference 59 describes an algebraic form of local atomic pseudopotentials for Al, Ga, and As that satisfy requirements (i)–(v) very well. We do not constrain the As pseudopotentials in AlAs and GaAs to be identical; thus we account for the different charge transfer in the two materials: after independently fitting the As pseudo-

potentials (denoted as $v_{\mathrm{As}}^{(0)}$ and $v_{\mathrm{As}}^{(4)}$, respectively) in GaAs and AlAs, the pseudopotential for As coordinated by $(4-n)$ Ga atoms and n Al atoms is taken as the weighted average

$$v_{\mathrm{As}}^{(n)}=\frac{4-n}{4}v_{\mathrm{As}}^{(0)}+\frac{n}{4}v_{\mathrm{As}}^{(4)} \ . \tag{8}$$

The analytic form and the parameters for the pseudopotentials are given in Ref. 59. As shown there, these atomic pseudopotentials for Ga, Al, and As provide excellent fits to the band structures, effective masses, deformation potentials, band offset, and work functions of GaAs and AlAs and of various ordered ternary compounds, including short-period and long-period superlattices.

C. Calculating the electronic structure of ~1000-atom structures

Having established structural models (Sec. II A) and defined pseudopotentials (Sec. II B) for our semiconductor alloys, we must next calculate the electronic structure. As discussed in Sec. II A, some of the special quasirandom structures used here involve unit cells with as many as 512 fcc sites (1024 atoms); our pseudopotentials require for these structures a plane-wave basis with as many as 30 000 orbitals. Band-structure calculations of such magnitude are extremely time consuming if conventional methods are used. The reason is that most approaches focus on the $\hat{H}\psi=\varepsilon\psi$ representation that forces one to calculate *all* eigensolutions below the physically most interesting ones [e.g., the valence-band maximum (VBM) or conduction-band minimum (CBM)]. For example, in a 1000-atom cell having 4000 electrons, the VBM is level number 2000 and the CBM is level 2001, yet conventional methods require that all 1999 levels below the VBM be calculated also, even if we are only interested in the value of the CBM−VBM band gap. This requirement (reflecting the need for orthogonality) leads to an overall N^3 scaling of the computational effort, thus limiting practical applications to ~100-atom systems. This problem can be circumvented if one is interested in eigensolutions only in an "energy window" (e.g., near the VBM and the CBM). In this case it is advantageous to use the alternative representation[60]

$$(\hat{H}-\varepsilon_{\mathrm{ref}})^2\psi_i=(\varepsilon_i-\varepsilon_{\mathrm{ref}})^2\psi_i \ , \tag{9}$$

where $\varepsilon_{\mathrm{ref}}$ is a "reference energy" selected in advance. The spectrum of the positive semidefinite operator $(\hat{H}-\varepsilon_{\mathrm{ref}})^2$ is the "folded spectrum" of $\hat{H}$ around $\varepsilon_{\mathrm{ref}}$. Therefore the lowest variational solution of Eq. (9) is the eigenstate with eigenenergy ε_i closest to $\varepsilon_{\mathrm{ref}}$. All eigenenergies of $\hat{H}$ below $\varepsilon_{\mathrm{ref}}$ are folded onto *positive* roots of Eq. (9). Hence, by placing $\varepsilon_{\mathrm{ref}}$ in the range of physical interest, one transforms an arbitrarily high eigensolution into the lowest one, thus obviating the need for orthogonalization to all other lower-lying eigenstates of $\hat{H}$. The computational effort scales only *linearly* with N, permitting large-scale calculations. In alloys, the most interesting levels are often those around the Fermi level. Thus, by placing $\varepsilon_{\mathrm{ref}}$ inside the energy gap, we find either the VBM or the CBM, depending on which is closer to $\varepsilon_{\mathrm{ref}}$. Changing $\varepsilon_{\mathrm{ref}}$ then assures that both levels are obtained. Usually, we calculate a small number of eigensolutions of Eq. (9) simultaneously. We expand ψ_i in plane waves, i.e., $\langle \mathbf{r}|\psi_i\rangle=\sum_{\mathbf{G}} C_i(\mathbf{G})e^{i\mathbf{G}\cdot\mathbf{r}}$. We then minimize $\langle\psi_i|(\hat{H}-\varepsilon_{\mathrm{ref}})^2|\psi_i\rangle$ using a preconditioned conjugate gradient method as described in Ref. 60. This method has been used successfully for empirical-pseudopotential-method (EPM) calculations on Si quantum dots containing ~2000 atoms.[60]

D. Spectral analysis of the electronic energy levels

The approach to the electronic structure of disordered alloys outlined in the previous sections is based on band theory of *periodic crystals* with large unit cells and low site symmetries. Here we show how to interpret such band structures while accounting for the absence of translational and rotational symmetry in a truly disordered alloy.

Measured optical spectra of $A_{1-x}B_xC$ zinc-blende alloys[61] are generally interpreted in the literature using the language of zinc-blende spectra; for example, the $\Gamma_{15v}\rightarrow\Gamma_{1c}$ transition of AC shifts continuously when BC is added to it. However, an energy level belonging to a particular (nontrivial) *irreducible representation* of the zinc-blende structure, such as Γ_{15} or X_1, does not lend itself to performing a configurational average in the sense of Eq. (2). This is because it is ill-defined for most of the 2^N possible configurations (e.g., a Γ_{15} state exists only in configurations of cubic symmetry).

Intuitively, the survival of zinc-blende-like features in the optical spectra of $A_{1-x}B_xC$ alloys follows from the fact that *on average* the disordered phase has the full zinc-blende symmetry. The naive virtual-crystal approximation exploits this fact by demanding that each and every atomic site in the alloy has the zinc-blende symmetry. In this unrealistic picture, all atoms on the mixed AB sublattice are replaced by identical, virtual atoms representing "chemical averages" of the two distinct atoms A and B. The virtual crystal thus has a well-defined band structure having the topology of the zinc-blende constituents AC and BC. Switching on the chemical differences between the atoms and allowing for atomic displacements results in a massive coupling between the VCA wave functions that have different band indices and wave vectors in the zinc-blende Brillouin zone. This leads to mixing of wave functions and level repulsion and results in optical bowing.[46]

The extent to which alloy electronic wave functions experience the average atomic crystal structure rather than a collection of local environments can be estimated quantitatively by projecting the wave functions of the alloy (represented, in principle, by a huge supercell, and in practice, by a SQS) on VCA states with zinc-blende symmetry. In fact, we can expand any alloy eigenstate $|\nu\rangle$ in terms of zinc-blende states $|n\mathbf{k}\rangle$ with band index n and wave vector $\mathbf{k}$ as

$$|\nu\rangle=\sum_{n,\mathbf{k}}|n\mathbf{k}\rangle\langle n\mathbf{k}|\nu\rangle \ . \tag{10}$$

The alloy states $|\nu\rangle$ with "signature" of a zinc-blende

state are those with dominant contribution in Eq. (10) from one particular state $|n\mathbf{k}\rangle$. We define the diagonal, symmetrized spectral density function[62] $A_{n,\sigma}(\mathbf{k},E)$ for configuration σ as

$$A_{n,\sigma}(\mathbf{k},E)=\frac{1}{N_R}\sum_{\hat{R},\nu(\sigma)}|\langle n,\hat{R}\mathbf{k}|\nu\rangle|^2\delta(E-E_\nu)\ , \quad (11)$$

where the sum runs over the N_R operations $\hat{R}$ of the zinc-blende point group, and over all electronic eigenstates $\nu(\sigma)$ of configuration σ with eigenvalue E_ν. An accurate theory of alloys would involve a sample with $N\rightarrow\infty$ sites, so its spectral function $A_{n,\infty}(\mathbf{k},E)$ will be a quasicontinuous function of E. The SQS approach can be thought of as sampling this spectral density at a finite number of wave vectors $\overline{\mathbf{K}}$ in the SQS Brillouin zone (we choose capital letters with overbar for these wave vectors to distinguish them from wave vectors in the zinc-blende Brillouin zone).

This discussion makes it clear that the quantity $P(\sigma)$ having a well-defined configurational average $\langle P\rangle$ [Eq. (2)] is the spectral density of Eq. (11). This is so because (i) the spectral density depends only on the configuration of atoms (through the Hamiltonian) and is defined for any configuration σ, and (ii) it is invariant under the space-group operations of the host lattice (by summing over all eigenstates). In the SQS approach, we approximate the configurational average by its SQS value, i.e., $\langle A_n(\mathbf{k},E)\rangle\approx A_{n,\mathrm{SQS}}(\mathbf{k},E)$. Hass, Davis, and Zunger[41] have shown that the spectral density obtained from a SQS-8 tight-binding calculation indeed yields a good approximation to a well-converged supercell calculation with $\sim$2000 atoms.

$\langle A_n(\mathbf{k},E)\rangle$ can be expanded in terms of its moments,[41] e.g., its first moment is the expectation value of the energy eigenvalue of $|n\mathbf{k}\rangle$ in the alloy,

$$\langle\varepsilon_n(\mathbf{k})\rangle=\frac{\int_{E_0}^{E_1}dE\,E\langle A_n(\mathbf{k},E)\rangle}{\int_{E_0}^{E_1}dE\langle A_n(\mathbf{k},E)\rangle}\ . \quad (12)$$

In principle, the integration limits are $E_0=-\infty$ and $E_1=\infty$. When several peaks are present in the spectral density, we calculate "restricted" moments in finite, nonoverlapping energy intervals $[E_0,E_1]$ around each peak. Comparing $\langle\varepsilon_n(\mathbf{k})\rangle$ with its unperturbed counterpart $\varepsilon_n(\mathbf{k})$ (from VCA or from the linear average of the constituent eigenvalues) gives us information about optical bowing, whereas the second moment of $\langle A_n(\mathbf{k},E)\rangle$ measures level broadening.

It is also desirable to make an analysis of SQS wave functions in real space, to gain information about their localized or delocalized nature. We do this by projecting the SQS wave functions on atomic spheres around each atom in the SQS unit cell. We use characteristic functions $|\psi_\Omega(\mathbf{r}_0)\rangle$ which are zero outside a sphere of volume Ω about origin $\mathbf{r}_0$ and $1/\Omega$ inside the sphere. A SQS wave function can then be projected on spheres centered on atoms belonging to a particular tetrahedral cluster $A_{4-n}B_n$. We define a cluster weight as

$$w_n(m\overline{\mathbf{K}})=\frac{1}{N_n}\sum_{\mathbf{r}_i}|\langle\chi_\Omega(\mathbf{r}_i)|m\overline{\mathbf{K}}\rangle|^2\ , \quad (13)$$

where N_n is the number of $A_{4-n}B_n$ clusters that occur in the SQS unit cell and $\mathbf{r}_i$ are the atomic positions in these clusters.

III. RESULTS

A. EPM results: Effects of SRO on the electronic properties of $Al_{0.5}Ga_{0.5}As$

The band gaps of the $Al_{0.5}Ga_{0.5}As$ alloy calculated using the spectral average defined in Eq. (12) for different degrees of SRO are presented in Table II. The total spectral weights included in the average are given in percentage. The agreement between the energies for SQS-N with $N=8$, 16, and 108 is typically better than 0.01 eV.

We start our discussion with the perfectly random alloy. Table II shows that the lowest gap in the random ($\alpha=0$) $Al_{0.5}Ga_{0.5}As$ alloy is indirect at X. The $\alpha=0$ spectral density functions from which the SQS-8 values in Table II are obtained are plotted in Figs. 2(a)–2(c), where the dotted line marks the average of the corresponding GaAs and AlAs band gap. As can be seen in Fig. 2(a), the Γ_{1c} transition shows considerable bowing and small mixing into states between 3.0 and 3.5 eV. Comparison with the spectral density of the (four equivalent) L_{1c} states shows [Fig. 2(c)] that both the bowing and the mixing with higher energy levels is similar to Γ_{1c} [Fig. 2(a)].

TABLE II. Band gaps (in eV) of the $Al_{0.5}Ga_{0.5}As$ alloy calculated by EPM using the spectral average [Eq. (12)] for different degrees of SRO. The total spectral weights are given in percentage. The fluctuations among different SQS-N are small when the included spectral weights are comparable (see the two lines for $\langle\Gamma_{1c}\rangle$). The shifts of the $\alpha=\frac{1}{6}$ SQS-108 energy gaps with respect to the random ones are given in the eighth column.

	Random ($\alpha=0$)			SRO ($\alpha=\frac{1}{6}$)			Shift (meV)
State	SQS-8	SQS-16	SQS-108	SQS-8	SQS-16	SQS-108	SQS-108
$\langle\Gamma_{1c}\rangle$		2.098 (69%)	2.119 (74%)	2.043 (64%)	2.039 (63%)	2.087 (71%)	−32
	2.167 (89%)	2.159 (88%)	2.129 (79%)	2.074 (79%)	2.075 (80%)	2.099 (75%)	−30
$\langle X_{1c}\rangle$	2.106 (99%)	2.108 (99%)	2.106 (99%)	2.091 (99%)	2.097 (99%)	2.098 (99%)	−8
$\langle L_{1c}\rangle$	2.229 (89%)	2.228 (89%)		2.215 (88%)	2.200 (85%)		−28

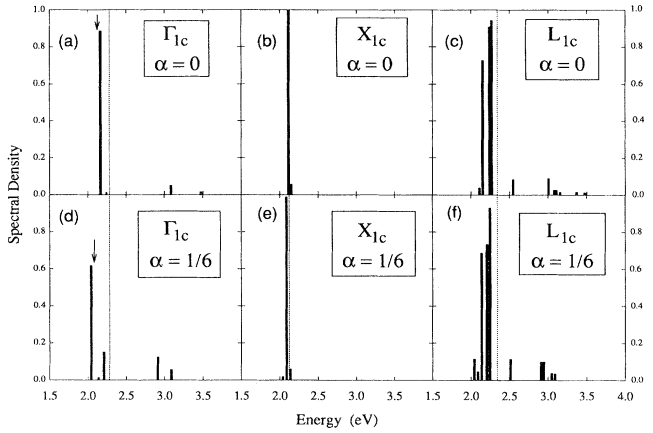

FIG. 2. EPM-calculated spectral densities of zinc-blende-like conduction states in the spectrum of $Al_{0.5}Ga_{0.5}As$ SQS-8 with (lower panel) and without (upper panel) SRO. The dotted vertical lines denote the corresponding average gaps of the binaries, and the arrows indicate the $\langle \Gamma_{1c} \rangle$ energy of SQS-108.

Projection of the SQS-8 wave functions on the corresponding VCA states reveals that the Γ_{1c} and L_{1c} states indeed couple. In contrast, the X_{1c} state shows virtually no bowing and very little mixing [Fig. 2(b)]. Optical bowing is usually quantified in terms of the bowing parameter b, defined as $E_g(x)=\bar{E}_g(x)-bx(1-x)$, where $\bar{E}_g(x)$ denotes the linear average of the band gaps of the constituents AC and BC at composition x. The $\alpha=0$ bowing coefficients calculated from band gaps in Table II are summarized and compared to experiment[63–67] and other theories[68] in Table III. We also give the compositions x_c at which the bands cross when bowing is taken into account. The agreement between the present EPM results and experiment is quite good for the Γ_{1c} bowing and the $\Gamma \rightarrow X$ and $X \rightarrow L$ crossover compositions. Discrepancies exist between our calculations and the rather uncertain experimental data[64] for the bowing of the L-like band gap. On the other hand, the agreement of the EPM results with LDA SQS-8 calculations (to be described below) is very good. This demonstrates again that the present EPM reproduces very well the wave-function coupling and level repulsion in ternary compounds with a variety of local atomic arrangements.

Introducing clustering-type SRO ($\alpha_1=\frac{1}{6}$) leads to stronger wave-function coupling, pushes the Γ_{1c} level down below the $\alpha=0$ value by ~ 80 meV, and broadens its spectral density [Table II and Fig. 2(d)]. Again, the L_{1c} state shows the same trend of increased bowing and level broadening [Fig. 2(f)]. Because X_{1c} is pushed down by only ~ 10 meV [Table II and Fig. 2(e)], the optical band gap of clustered $Al_{0.5}Ga_{0.5}As$ is now *direct*. Thus we predict an indirect-to-direct crossover in $Al_{0.5}Ga_{0.5}As$ with sufficient local clustering.

We next analyze the effects of SRO on the wave functions of the lowest conduction and highest valence states. Figure 3 shows histograms of the cluster weights w_n [Eq. (13)] measuring the probability to find a wave function on an $Al_{4-n}Ga_n$ cluster in the alloy. As the degree α of SRO increases, the number of *both* Ga_4 and Al_4 clusters increases in the alloy by the same amount, while the number of mixed clusters ($n=1,2,3$) decreases (see the Appendix). Figure 3 shows that as SRO sets in, the wave functions at the conduction-band edge strongly localize on the Ga_4 clusters, while the corresponding states in the random alloy are spread over all cluster types. Comparing the large SQS-N results with those of SQS-8 and SQS-16 in Fig. 3, we see that the smaller SQS's tend to exaggerate the degree of localization, but in all cases clus-

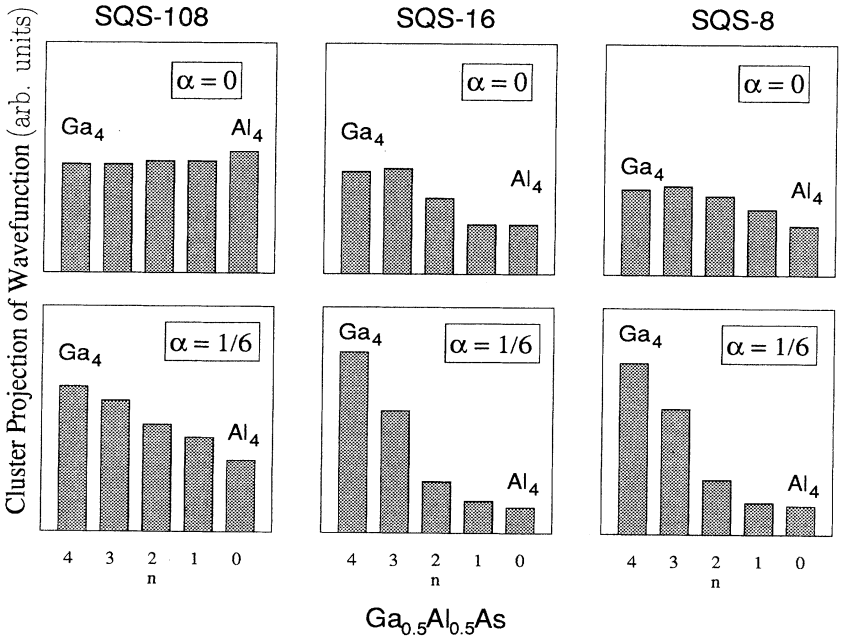

FIG. 3. EPM-calculated cluster projections [Eq. (13)] of the CBM wave function on $Al_{4-n}Ga_n$ clusters in $Al_{0.5}Ga_{0.5}As$ SQS-N, with $N=8,16,108$, with (lower panel) and without (upper panel) SRO. The units are arbitrary but have the same scale for each N, and the individual columns are normalized to one cluster. The atomic sphere volumes Ω used for the projections are equal to the average atomic volume in the alloy.

TABLE III. Band gaps E_g, bowing coefficients b (in eV), and critical crossover compositions x_c of the $Al_{1-x}Ga_xAs$ alloy. EPM band gaps are from Table II. LDA conduction-band eigenvalues have been rigidly shifted by 0.84 eV to agree with experimental band gaps of the binaries. $\bar{E}_g$ is the 50%-50% average band gap of AlAs and GaAs. Experimental band gaps are low-temperature values; bowing coefficients were measured at various temperatures.

	Present EPM SQS-16	Experiment	LDA SQS-8	CPA[a]
$\bar{E}_g(x=\frac{1}{2})$ (eV)	2.12	2.12	2.18	
	Random			
$E_g(x=\frac{1}{2})$ (X_{1c})	2.11	2.08[b]	2.17	
$b(\Gamma_{1c})$	0.48	0.37[c]	0.23	0.27
$b(X_{1c})$	0.05	0.15[d]	0.04	0.18
$b(L_{1c})$	0.45	0.055[c]	0.33	0.20
$x_c(\Gamma\rightarrow X)$	0.46	0.41[e]–0.43[f]	0.47	
$x_c(L\rightarrow X)$	0.34	0.35[f]	0.35	
$x_c(\Gamma\rightarrow L)$	0.65	0.47[f]	0.88	
	With SRO $\alpha=\frac{1}{6}$			
$E_g(x=\frac{1}{2})$ (Γ_{1c})	2.08		2.13	
$b(\Gamma_{1c})$	0.81		0.58	
$b(X_{1c})$	0.09		0.11	
$b(L_{1c})$	0.56		0.45	
$x_c(\Gamma\rightarrow X)$	0.52		0.51	
$x_c(L\rightarrow X)$	0.37		0.35	
$x_c(\Gamma\rightarrow L)$	0.74		0.94	

[a]Reference 68.
[b]Reference 63.
[c]Reference 64.
[d]Reference 65.
[e]Reference 66.
[f]Reference 67.

tering leads to localization on Ga. We will see in Sec. III C how this localization correlates with atomic s-orbital energies of the cations.

B. LDA results: Effects of SRO on the electronic properties of $Al_{0.5}Ga_{0.5}As$, $Ga_{0.5}In_{0.5}P$, and $Al_{0.5}In_{0.5}As$

For structures up to SQS-16, i.e., 32 atoms per unit cell, we use finite-principles pseudopotentials in addition to the empirical ones. This allows us to study the charge transfer and its effect on the electronic structure in different atomic environments in a self-consistent manner. We construct the nonlocal pseudopotentials using the approach of Kerker.[69] Exchange and correlation effects are treated in the local-density approximation using the Ceperley and Alder[70] potential in the parametrization of Perdew and Zunger.[71] The kinetic-energy cutoff for the plane waves is 15 Ry, and Brillouin-zone integrations are done using an equivalent of 29 special **k** points of the fcc structure.[72,73] As is well known,[71] LDA calculations severely underestimate conduction-band energies. To compare our results to experimental and EPM results, we *rigidly* shift the LDA conduction energy eigenvalues by an amount depending on the constituents and composition of the alloys.[74] The $Ga_{0.5}In_{0.5}P$ and $Al_{0.5}In_{0.5}As$ supercell geometries have been determined with VFF, as described in Sec. II A.

The LDA results for $Al_{0.5}Ga_{0.5}As$ have been compared with the EPM results in Table III. The conclusions drawn from the EPM calculations in Sec. III A are confirmed by the LDA calculations.

We now extend the theory to $Ga_{1-x}In_xP$ and $Al_{1-x}In_xAs$. The optical bowing obtained from the random SQS-16 band structure of $Ga_{0.5}In_{0.5}P$ is $b=0.46$ eV (tight-binding s-CPA gives[68] $b=0.52$ eV). Strong clustering ($\alpha=\frac{1}{6}$) reduces the gap even further, as in the case of $Al_{0.5}Ga_{0.5}As$. The resulting bowing coefficient in the presence of clustering is $b=0.90$ eV. The experimental values range from 0.50 to 0.79 eV (Ref. 75). The relatively wide scattered experimental data make it difficult to draw conclusions on the possible presence of SRO in the experimental samples, even though in the light of our theory larger bowing parameters would seem to indicate clustering-type SRO. However, different experimental techniques and the models employed to extract bowing parameters can also be responsible for the scattering of the data. To clarify this issue, independent, direct measurements of SRO on the same samples are needed. Like $Al_{1-x}Ga_xAs$, $Ga_{1-x}In_xP$ is an alloy of a direct-gap (InP) and an indirect-gap (GaP) material. At composition $x=0.5$, however, the random $Ga_{1-x}In_xP$ alloy is direct, and cation clustering does not change the nature of the band gap, as is the case for $Al_{0.5}Ga_{0.5}As$. Nevertheless, strong clustering can reduce the direct band gap considerably.

We have also performed a spectral analysis of the electronic structure of the SQS-8 with *anticlustering*[52] SRO ($\alpha=-\frac{1}{6}$). We find no significant difference with respect to the $\alpha=0$ alloy, i.e., no additional bowing or localization of the wave functions as in the case of clustering-type SRO. We conclude that nearest-neighbor ordering-type SRO leaves no fingerprints on the near-band-gap optical spectra of III-V alloys.

We obtain similar results for $Al_{1-x}In_xAs$. Like $Al_{1-x}Ga_xAs$, this alloy is made of an indirect-gap (AlAs) and a direct-gap (InAs) component. The bowing coefficient for the random $Al_{0.5}In_{0.5}As$ alloy is calculated as $b=0.52$ eV. Upon clustering ($\alpha=\frac{1}{6}$), the bowing coefficient increases to $b=0.88$ eV. The experimental values are 0.24 eV (Ref. 75) and 0.74 eV (Ref. 76); tight-binding s-CPA gives[68] $b=0.70$ eV.

The spectral density function defined in Eq. (11) is directly related to the oscillator strength of a given transition in the alloy. This can be seen by taking the dipole matrix element between two alloy states expanded in terms of zinc-blende states [Eq. (10)] and recognizing that only a few zinc-blende dipole matrix elements will contribute to the expansion of the alloy matrix element. Indeed, when calculating the dipole matrix elements between an SQS valence- and conduction-band wave function, we found that it was directly proportional to the Γ_{1c} projection of the conduction state. In other words, even if a zinc-blende conduction state away from the Brillouin-zone center is mixed into the zone center wave functions by alloying, it does not contribute to optical

transitions from the VBM. This is analogous to the observation that "folded," or pseudodirect, transitions in superlattices carry almost no oscillator strength.

We now compare the SRO effects on the alloy band structure with those caused by LRO. In the presence of LRO (Fig. 4), the spectral density is strikingly different from that in the presence of SRO (Fig. 2). In the fully ordered CuPt structure, the Γ_{1c} and folded L_{1c} strongly intermix and form two $\overline{\Gamma}_{1c}$ states of $\sim 50\%$ Γ_{1c} and $\sim 50\%$ L_{1c} character.[5,77] The spectral function $A_{1c,\mathrm{CuPt}}(\overline{\Gamma},E)$ therefore has two peaks of about equal height [Fig. 4(c)]. Associated with the Γ-L mixing is a spatial segregation of the lower $\overline{\Gamma}_{1c}$ state on the Ga(111) planes[77] and of the higher $\overline{\Gamma}_{1c}$ state on the In(111) planes. The band-gap reduction with respect to the random alloy associated with this level repulsion is 0.23 and 0.34 eV for $\eta=\frac{1}{2}$ and $1/\sqrt{2}$, respectively, and 0.49 eV for $\eta=1$. The band-gap reduction as a function of the LRO parameter η is often used to determine η by measuring the band gap.[1] From our results on SRO above we now know that clustering can also lead to a band-gap reduction. If SRO and LRO coexist in the same sample, the band-gap reduction could be partially caused by SRO, and great care has to be taken when "inverting" the band-gap vs η relation. Crystal-field splitting, which is not affected by SRO, is an optical probe of LRO (and strain) alone, and can therefore remove some of the ambiguity.[78]

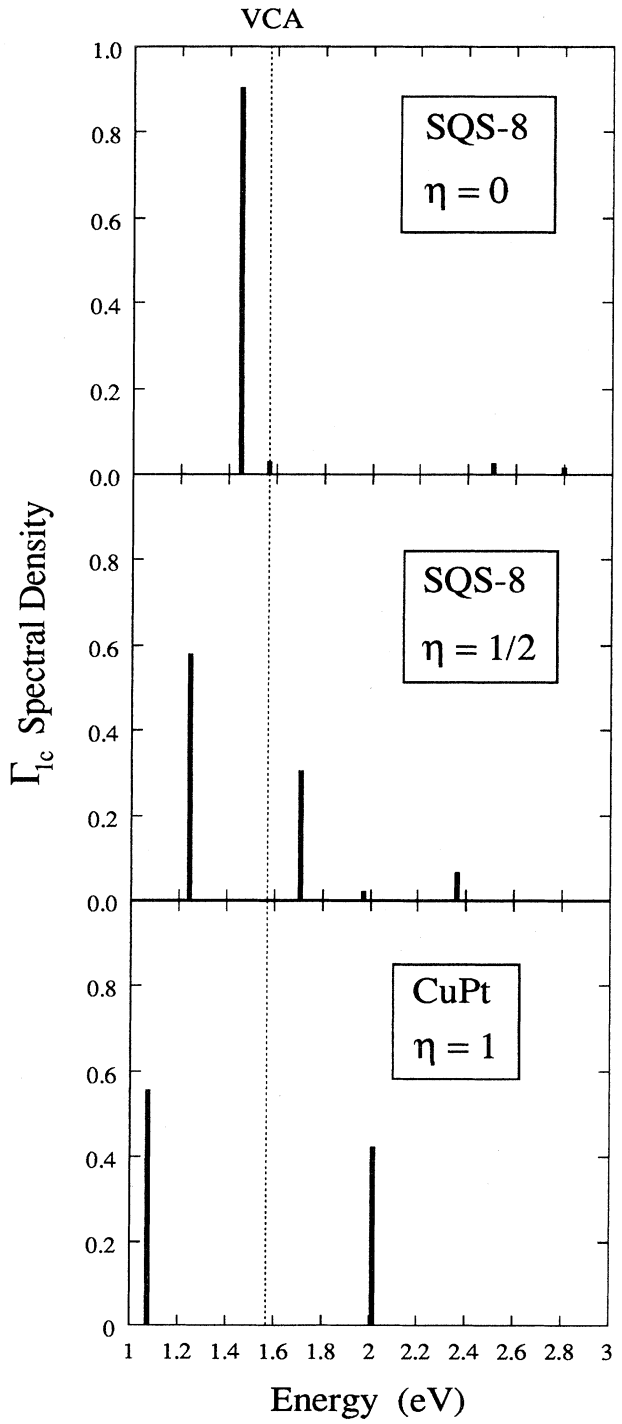

FIG. 4. LDA-calculated spectral density of the zinc-blende-like Γ_{1c} state in $Ga_{0.5}In_{0.5}P$ with CuPt-like LRO. For $\eta=0$ and $\eta=\frac{1}{2}$, we use SQS-8; for $\eta=1$ we use the four-atom CuPt unit cell. Energies are uncorrected LDA results.

The LDA-corrected results for the band gaps of $Al_{0.5}Ga_{0.5}As$, $Ga_{0.5}In_{0.5}P$, and $Al_{0.5}In_{0.5}As$ with SRO and LRO are summarized in Table IV and are compared to the random alloy values and the linear averages of the constituents. Table IV also shows on which types of clusters (planes) the band-edge wave functions are localized in the presence of SRO (LRO). For the CBM of $Al_{0.5}Ga_{0.5}As$ and $Ga_{0.5}In_{0.5}P$, as well as the VBM of $Al_{0.5}In_{0.5}As$ in the presence of SRO, the wave-function localization is illustrated in Fig. 1 of Ref. 39. There, the LDA-calculated cluster projections [Eq. (13)] of these band-edge wave functions are shown (compare with the EPM-calculated results in Fig. 3), together with contour plots in a plane which intersects both an A_4 and a B_4 cluster.

C. Discussion: Physical mechanism and chemical trends

Our results presented above show that clustering on the cation sublattice of $Al_{0.5}Ga_{0.5}As$, $Ga_{0.5}In_{0.5}P$, and $Al_{0.5}In_{0.5}As$ alloys leads to (i) strong enhancement of the optical bowing of the direct band gap and (ii) localization of the VBM and/or CBM wave function on one type of cluster (Fig. 3 and Table IV). Observations (i) and (ii) are related as follows. We have seen that the enhancement of optical bowing with clustering reflects a stronger mixing of wave functions with different wave vectors in the zinc-blende Brillouin zone (see Fig. 2). This, in turn, means that in the presence of clustering, the alloy wave functions are composed of a wider distribution of zinc-blende states in $\mathbf{k}$ space [Eq. (10)], and hence are more localized in real space. What is the mechanism leading to wave-function localization, or equivalently, to strong wave-vector mixing? We will answer this question using two complementary physical pictures: (i) the "impurity picture," where we emphasize the local nature of the potential change when atoms are substituted and small clusters are formed, and (ii) the "quantum-well picture," where the bulk properties of domains of pure constituents are

TABLE IV. LDA-corrected band gaps in eV (measured from the top of the valence band) for three alloy systems at different states of order: perfect randomness ($\alpha=\eta=0$), clustering-type SRO ($\alpha=\frac{1}{6}$), and CuPt-type LRO ($\eta=1$). Here, $\bar{E}_g$ denotes the average gap of the binaries at their equilibrium volumes. Chemical symbols in parentheses denote the sublattice on which the VBM and CBM are localized, respectively, and D denotes that the state is delocalized.

System		$\bar{E}_g$	Random	SRO $\alpha=\frac{1}{6}$		LRO $\eta=1$	
$Al_{0.5}Ga_{0.5}As$	Γ_{1c}	2.27	2.22	2.13	(Ga/Ga)	1.86	(D/Ga)
	X_{1c}	2.18	2.17	2.16		2.10	
$Ga_{0.5}In_{0.5}P$	Γ_{1c}	2.16	2.06	1.93	(In/Ga)	1.57	(In/Ga)
$Al_{0.5}In_{0.5}As$	Γ_{1c}	1.78	1.65	1.56	(In/D)	1.49	(In/D)

used to describe the wave-function localization in clustering alloys.

1. *Impurity picture of carrier localization in clustered alloys*

We first consider the CBM. The CBM wave function in $Al_{0.5}Ga_{0.5}As$ and $Ga_{0.5}In_{0.5}P$ is strongly localized on Ga-rich clusters (Table IV). In $Al_{0.5}In_{0.5}As$, the CBM is weakly localized on the In-rich clusters. The chemical trend pertinent to this observation follows the order of atomic s-orbital energies, which increase in the sequence Ga→In→Al (LDA values are −9.16, −8.46, and −7.83 eV, respectively). Because the CBM wave functions in the clustered alloys are mostly s-like (they derive mainly from Γ_{1c}), this correlation implies that the clusters act as "impuritylike traps": it is well known that an isolated isoelectronic impurity binds a carrier if the difference between its local potential and that of the host atom exceeds a critical value.[79] An *isolated* Ga impurity in an AlAs or InP host crystal is not strong enough to bind an electron.[80] Because the strength of the local potential is determined by its depth as well as its range, a natural question arises: At what critical size n will an A_n *cluster* in a *BC* host crystal show a bound state? To investigate this question, we have performed EPM calculations on AlAs supercells containing 512 atoms where a cluster of n Al atoms is substituted by Ga atoms.[59] The case of $Al_{1-x}Ga_xAs$ is particularly simple because there is no size mismatch between GaAs and AlAs, and the local potential differences between Al and Ga reflect purely chemical differences. Our findings are[59] (i) A Ga_n cluster in an AlAs host with $n \leq 14$, produces Γ-like *resonances* within the conduction bands of AlAs, but no gap states. The Γ-like and L-like resonances for $n=1$ and 4 are close in energy to the corresponding conduction states in an $Al_{1-x}Ga_xAs$ alloy of the same composition as the supercell ($x=n/256$), whereas for $n=14$ they are about 150 meV below their "parent states." (ii) Although a single Ga_4 cluster does not produce a bound state, a finite concentration of such clusters, present in our $\alpha=\frac{1}{6}$ SQS, pushes the resonant levels down further, leading to a Γ-like CBM in $Al_{0.5}Ga_{0.5}As$ with wave-function localization on Ga-rich clusters (cf. Table IV and Fig. 3). Thus it is the existence of a finite concentration of small clusters embedded in the alloy medium[81] that causes wave-function localization and band tailing, much like in the substitutional alloy theory of Lifshitz.[82]

2. *Quantum-well picture of carrier localization in clustered alloys*

In $Ga_{0.5}In_{0.5}P$ and $Al_{0.5}In_{0.5}As$, in addition to purely chemical differences between the atomic (pseudo)potentials, the size mismatch between the cations leads to local strain in the crystal lattice. The lattice relaxation will considerably modify the perturbation introduced by the chemical difference of the substituted atoms.[79] The importance of this effect is illustrated in Fig. 5, where an energy-level diagram is plotted for the GaP/InP system. We compare the energy levels of GaP and InP at their respective equilibrium volume V_{eq} with those at the $Ga_{0.5}In_{0.5}P$ alloy volume $\bar{V}$. In the case of coherent phase separation, each constituent is constrained to the fixed volume $\bar{V}$: GaP is hydrostatically expanded and InP is hydrostatically compressed. The

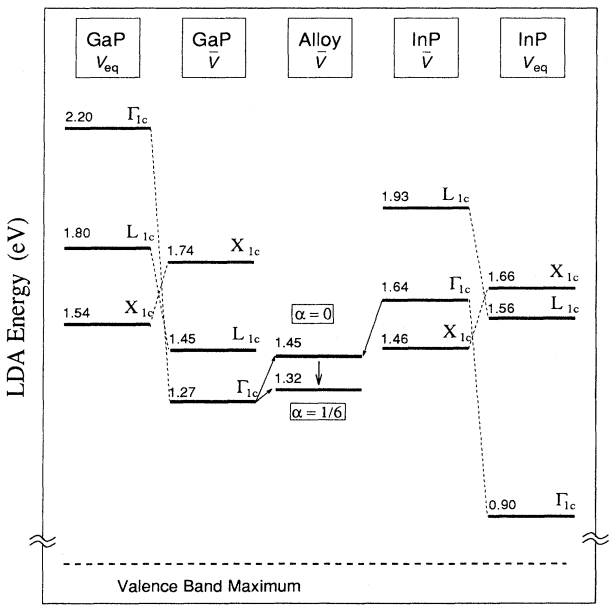

FIG. 5. Band-gap diagram of the GaP/InP system (LDA eigenvalues in eV) assuming a zero valence-band offset. The band gaps of GaP and InP bulk are given both at their equilibrium volume V_{eq} and at the volume of the $Ga_{0.5}In_{0.5}P$ alloy $\bar{V}$. For the alloy, the lowest conduction states of SQS-8 with and without SRO are given.

changes in the energy spectrum—as described by the *hydrostatic* deformation potentials—is dramatic: GaP transforms from an indirect-gap material at X to a direct-gap material, whereas InP transforms from a direct-gap material to an indirect-gap material at X (Fig. 5). Therefore, in the coherently phase-separated GaP/InP system, the CBM is localized on GaP, rather than on InP, as would be the case if the constituents would relax to their respective equilibrium volume (incoherent phase separation). This establishes the "quantum-well picture," where the electrons are assumed to obey an effective-mass-like Schrödinger equation with the potential given by the properly lined-up band edges. In Fig. 5, the CBM of the $\alpha=0$ and $\frac{1}{6}$ alloy are also shown, as obtained from SQS-8. Note that localization of the CBM wave function in the clustered alloy on Ga agrees with both the impurity picture with its s-orbital rule outlined above, as well as the quantum-well picture (valid when coherent phase separation is complete, and illustrated in Fig. 5). This qualitative agreement is not obvious, and the evolution of the electronic spectrum when going from a single isoelectronic impurity via a cluster (or quantum dot) to bulklike domains in a host crystal is not well studied at present.

3. *Hole localization*

So far we have discussed conduction-band (or electron) localization. The physical mechanism leading to localization of the VBM (or hole) wave function is qualitatively similar. We have to consider whether an isoelectronic substitution is attractive or repulsive to holes. The holes at the VBM in the III-V semiconductors are p-like and segregated mostly on the *anion sublattice.* The p-orbital energies in the free Al, Ga, and In atoms are almost equal. Nevertheless, it was shown by Wei and Zunger[83] that the relative position of the Γ_{15v} state in III-V common-anion systems is mostly determined by p-d repulsion of the *cation* orbitals. Because in Al the d orbitals lie above the p orbitals, the Γ_{15v} states in the Al binaries are expected to be pushed below the ones in the Ga and In binaries, where the orbital order is opposite.[83] Therefore the p-d repulsion argument suggests that the holes will localize on Ga and In clusters in $Al_{1-x}Ga_xAs$ and $Al_{1-x}In_xAs$ alloys, respectively. The predictions of this simple two-level model indeed agree with the direct calculations on clustered alloys, as shown in Table IV. In a common-anion Ga/In system, p-d repulsion alone does not give a clear indication where the holes are expected to be localized. Let us use the quantum-well picture instead. We need the valence-band offsets between the constituents (assumed to be zero in Fig. 5) hydrostatically strained to the alloy volume $\bar{V}$. This allows us to predict where the holes will be localized when coherent phase separation occurs. In AlAs/GaAs, the VBM in GaAs is about 0.50 eV higher[84] than that of AlAs. The valence-band offset in hydrostatically strained AlAs/InAs is not directly available, but it can be estimated from the epitaxial AlAs/InAs (001) system, where *uniaxial strain* applies. The offset of the crystal-field and spin-orbit-averaged VBM has been calculated[85] to be ~ 0.45 eV, and the VBM of InAs to be higher than that of AlAs. Upon hydrostatic expansion of AlAs and compression of InAs, the VBM of InAs is expected[86] to increase with respect to AlAs. Therefore, in AlAs/InAs, the VBM in InAs will be higher by $\gtrsim 0.50$ eV than that in AlAs. Similarly, linear-augmented-plane-wave calculations[86] indicate that in GaP/InP the VBM will be on InP. The hole localization in coherently phase-separated $Al_{0.5}Ga_{0.5}As$, $Ga_{0.5}In_{0.5}P$, and $Al_{0.5}In_{0.5}As$ is therefore expected to be on GaAs, InP, and InAs domains, respectively. Again, this is in agreement with our findings for the clustered alloys, as shown in the sixth column of Table IV. The quantum-well picture works surprisingly well, even when the phase separation is limited to nearest-neighbor shells.

IV. CONCLUSIONS

We have presented a method to study the electronic structure of pseudobinary semiconductor alloys with a given degree of short-range order. The method accounts in a statistically accurate fashion for a *distribution* of local atomic environments and thus goes beyond mean-field treatments of alloys. Special configurations of $8 \leq N \lesssim 500$ lattice sites were constructed that mimic much larger supercells and thus allow for the calculation of configurational averages with a *single calculation* of manageable computational effort. For large supercells, a simulated-annealing technique is used to find an atomic configuration that corresponds to the desired ordering state (random or short-range order). Whereas self-consistent LDA calculations are practical for structures with up to ~ 32 atoms per unit cell, we have used the empirical pseudopotential method for structures with ~ 1000 atoms per unit cell. An efficient algorithm, whose effort scales linearly with system size, allowed us to directly calculate the band-edge wave functions for these large supercells without solving first for all lower-lying states. We have described in detail how to analyze the electronic energy-level spectrum of the "special" structures and obtain properly defined configurational averages pertinent to the electronic structure of the ideal alloys they represent. We have proven that the spectral density function of a zinc-blende state in the alloy spectrum has a well-defined configurational average and that this average can be approximated by the extended SQS method.

We have studied the band gaps of $Al_{1-x}Ga_xAs$, $Ga_{1-x}In_xP$, and $Al_{1-x}In_xAs$ alloys, with and without short-range order. Our main findings are the following.

(i) Optical bowing, present in the random alloy, is enhanced by clustering. Band gaps are lowered by as much as 100 meV in the presence of strong nearest-neighbor clustering. Local ordering (anticlustering), on the other hand, does not change much the band gaps of these alloys. The large scattering of experimental data on bowing parameters could in part be due to clustering, although other sources of uncertainties are very likely to be equally important.

(ii) In the case of $Al_{0.5}Ga_{0.5}As$, we predict an indirect-

to-direct band-gap crossover with sufficiently strong clustering.

(iii) The large band-gap reductions are accompanied by localization of the band-edge wave functions on particular types of clusters. Electrons at the conduction-band minimum are localized on Ga clusters in $Al_{0.5}Ga_{0.5}As$ and $Ga_{0.5}In_{0.5}P$, and holes at the valence-band maximum are localized on Ga clusters in $Al_{0.5}Ga_{0.5}As$ and on In clusters in $Ga_{0.5}In_{0.5}P$ and $Al_{0.5}In_{0.5}As$. We have explained this phenomenon in terms of (i) an impurity picture, where the alloy is viewed as a host with randomly distributed or clustered isoelectronic substitutional impurities, and (ii) a quantum-well picture, which considers the limit of coherent phase separation with formation of hydrostatically strained domains of the constituent materials. We have shown that both pictures are consistent with our results. In particular, approach (i) implies an *s*-orbital rule for electron localization: the wave function at the conduction-band minimum is localized on clusters of the cation with lower *s*-orbital energy. The localization of VBM wave functions in AlX/GaX and AlX/InX alloys (X denoting the common anion) follows the trend of *p-d* repulsion: Al impurities and clusters are repulsive to holes, and therefore the holes are localized on Ga or In clusters.

(iv) Our findings for gap reduction in clustered alloys have been compared to alloys which exhibit long-range order. Although in both cases the band-gap reduction with respect to the random alloy can be large, i.e., a few tenths of an eV, the mechanisms leading to the gap reduction are quite different. In the case of LRO, the gap reduction is the result of level repulsion between a small number of states that are coupled through the Fourier components of the ordering potential taken at the reciprocal lattice vectors of the fully ordered structure, whereas SRO has no translational symmetry. Moreover, the LRO-induced gap reduction increases monotonically with the LRO parameter η. In experiments relating the band-gap reduction to η, the presence of clustering needs to be taken into account as a possible source of a portion of band-gap narrowing.

(v) We reported band gaps for CuPt-ordered $AlGaAs_2$, $GaInP_2$, and $AlInAs_2$, which provide useful information for correlating optical data with the LRO parameter in partially ordered alloys.

(vi) Our results on bond lengths in random $Ga_{0.5}In_{0.5}P$ are in excellent agreement with extended x-ray-absorption fine-structure measurements. In clustered alloys, we find that cation-anion bond lengths deviate more from their zinc-blende value than in the random alloy, thus increasing the strain energy. In $Ga_{0.5}In_{0.5}P$ the short Ga-P bond elongates relative to the random alloy value, while the longer In-P bond shortens.

ACKNOWLEDGMENTS

We thank Dr. S.-H. Wei, Dr. L.-W. Wang, and Dr. S. Froyen for stimulating discussions and helpful contributions. This work was supported by the Office of Energy Research, Materials Science Division, U.S. Department of Energy, under Grant No. DE-AC02-83CH10093.

APPENDIX: QUALITY OF PRESENT SQS'S

The quality of a SQS can be quantified in terms of Q_s, defined in Eq. (7), which measures differences between $\overline{\Pi}_f$(SQS) and the "ideal" $\langle \overline{\Pi}_f \rangle$. In the case of SRO, the ideal pair-correlation functions are determined from Eq. (5), and in the case of LRO, they are determined from Eq. (6). The weights w_f in Eq. (7) are chosen to be $w_f = 2^{-(k_f-2)} m^{-1}$, where k_f is the number of vertices and m is the order of the largest shell in figure $f=(k_f,m)$. Including in Eq. (7) pair figures up to the seventh shell and nearest-neighbor triplets and quadruplets, we obtain quality coefficients Q_s of 0.920, 0.000, 0.073, and 0.000 for the random SQS-8, SQS-16, SQS-108, and SQS-512, respectively. Note the excellent quality of $\alpha=0$ SQS-16, which is actually superior to the best SQS-108 (constrained to a unit cell of cubic shape) found by simulated annealing. Similar results apply for the nonrandom SQS's.

The number of tetrahedral $A_{4-n}B_n$ ($n=0,1,2,3,4$) clusters in the $\alpha=0$ and $\alpha=\frac{1}{6}$ SQS's is shown in Table V. For comparison, we also give the values for the large (512 fcc site) SQS which are nearly exact. Their distribution is linearly related to the composition x and the $\overline{\Pi}_f$ of the nearest-neighbor pair, triplet, and quadruplet figures. For the random alloy, they obey a binomial distribution. For clustering SRO, the relative number of the pure clusters A_4 and B_4 increases at the expense of the mixed clusters (see lower part of Table V).

A further test of the statistical quality of the SQS's consists of counting the numbers O_m of atoms of opposite type in the mth neighbor shell of each atom in the unit cell. For the random alloy, the configuration average $\langle O_m \rangle$ and its variance have been derived analytically by Wei *et al.*[47] and compared to SQS-8. More generally, one can show that

$$\langle O_m \rangle = D_m (1 - \langle \overline{\Pi}_{(2,m)} \rangle) , \tag{A1}$$

where D_m is the degeneracy of pair figure $f=(2,m)$. For pair figures, D_m is half the number of sites (coordination number) in the mth shell. For the random alloy, for which $\langle \overline{\Pi}_{(2,m)} \rangle = 0$, Eq. (A1) reduces to Eq. (A11) in the

TABLE V. The number of fcc nearest-neighbor tetrahedral clusters A_nB_{4-n} present in SQS-N for composition $x=\frac{1}{2}$. The relative numbers of clusters are normalized to a total of 32 clusters. Note that in SQS-N, there are $2N$ tetrahedral clusters per unit cell. The exact number of clusters for $\alpha \neq 0$ is not known, since the triplet and quadruplet correlation functions are not determined by SRO. The description of these structures is given in Ref. 52.

SRO	SQS-N	A_4	A_3B	A_2B_2	AB_3	B_4
$\alpha=0$	SQS-8($a+b$)	2	8	12	8	2
	SQS-16	2	8	12	8	2
	SQS-512	2	8	12	8	2
	Exact	2	8	12	8	2
$\alpha=+\frac{1}{6}$	SQS-8	4	8	8	8	4
	SQS-512	4.08	7.64	8.56	7.64	4.08

TABLE VI. Average $\langle O_m \rangle_N$ and its standard deviation of the number of mth shell neighbors of opposite type in SQS-N and the corresponding value $\langle O_m \rangle_\infty$ in an ideal *infinite* cell [Eqs. (A1) and (A2)]. N_C denotes the shell coordination number.

	Number of opposite neighbors in SQS-N						
	First shell $N_C=12$	Second shell $N_C=6$	Third shell $N_C=24$	Fourth shell $N_C=12$	Fifth shell $N_C=24$	Sixth shell $N_C=8$	Seventh shell $N_C=48$
			SQS-8 with $\alpha=0$ (random alloy)				
$\langle O_m \rangle_8$	6±1.8	3±0.5	11.5±1.1	6.5±0.5	11±1.4	4±1	27±3
$\langle O_m \rangle_{512}$	6±1.7	3±1.2	12±2.4	6±1.7	12±2.3	4±1.4	24±3.5
$\langle O_m \rangle_\infty$	6±1.7	3±1.2	12±2.4	6±1.7	12±2.4	4±1.4	24±3.5
			SQS-8 with $\alpha_1=-\frac{1}{6}$				
$\langle O_m \rangle_8$	7±0	3±0	12±0	6±0	10±0	4±0	24±0
$\langle O_m \rangle_{512}$	7±0.8	3±1.2	11.3±1.9	6±1.7	12±1.9	4±1.3	24±2.8
$\langle O_m \rangle_\infty$	7±1	3±1.2	12±2	6±1.7	12±2	4±1.4	24±2.8
			SQS-8 with $\alpha_1=+\frac{1}{6}$				
$\langle O_m \rangle_8$	5±2	3±0	12±0	6±0	14±4	4±0	24±0
$\langle O_m \rangle_{512}$	5±2.0	3±1.2	12±2.8	6±1.7	12±2.5	4±1.3	24±3.7
$\langle O_m \rangle_\infty$	5±2.2	3±1.2	12±2.8	6±1.7	12±2.8	4±1.4	24±4

Appendix of Ref. 47. In the presence of SRO, Eq. (5) can be used to find $\langle O_m \rangle$ for given SRO parameters α_m. For the variance of $\langle O_m \rangle$ we obtain

$$\langle O_m^2 \rangle - \langle O_m \rangle^2 = \tfrac{1}{2} D_m \left[1 + \sum_j d_m(j) \alpha_j \right] , \qquad \text{(A2)}$$

where $d_m(j)$ is the number of jth nearest neighbors per atom which belong to the same mth neighbor shell. In other words, $d_m(j)$ is the intersection of the mth shell and the jth shell with its origin on the former. For example, in the nearest-neighbor shell ($m=1$), each atom has 4 out of 12 nearest neighbors which also belong to the same shell, therefore $d_1(1)=4$. If only $\alpha_1 \neq 0$, as in the present study of SRO, we need $d_m(1)$ to calculate the standard deviation of $\langle O_m \rangle$ [square root of Eq. (A2)]. The ideal values, as calculated from Eqs. (A1) and (A2), are compared with the corresponding *lattice averages* of O_m in the SQS in Table VI. The SQS errors in $\langle O_m \rangle$ are proportional to the errors in $\overline{\Pi}_{(2,m)}$, but comparing the standard deviations of $\langle O_m \rangle$ provides an additional test of quality. Whereas the $\alpha=\pm\frac{1}{6}$ SQS-8 have rather large errors in some of the standard deviations, the $\alpha=0$ SQS-8 shows better agreement with the ideal values. In all cases, the SQS-512 reproduces very well the statistics of an infinite sample.

[1]For a review, see A. Zunger and S. Mahajan, *Atomic Ordering and Phase Separation in Epitaxial III-V Alloys,* 2nd ed., Handbook on Semiconductors Vol. 3 (Elsevier, Amsterdam, 1994).

[2]A. Gomyo, K. Kobayashi, S. Kawata, I. Hino, and T. Suzuki, J. Cryst. Growth **77**, 367 (1986).

[3]M. Kondow, H. Kakibayashi, and S. Minagawa, J. Cryst. Growth **88**, 291 (1988); M. Kondow, H. Kakibayashi, S. Minagawa, Y. Inoue, T. Nishino, and Y. Hamakawa, *ibid.* **93**, 412 (1988); M. Kondow and S. Minagawa, Appl. Phys. Lett. **54**, 1760 (1989).

[4]D. J. Arent, M. Bode, K. A. Bertness, S. R. Kurtz, and J. M. Olson, Appl. Phys. Lett. **62**, 1086 (1993).

[5]S.-H. Wei and A. Zunger, Phys. Rev. B **39**, 3279 (1989).

[6]D. B. Laks, S.-H. Wei, and A. Zunger, Phys. Rev. Lett. **69**, 3766 (1992).

[7]J. M. Cowley, J. Appl. Phys. **21**, 24 (1950).

[8]L. G. Ferreira, S.-H. Wei, and A. Zunger, Phys. Rev. B **40**, 3197 (1989).

[9]S.-H. Wei, L. G. Ferreira, and A. Zunger, Phys. Rev. B **41**, 8240 (1990).

[10]V. T. Bublik, M. B. Karman, V. F. Kleptsin, and V. N. Leikin, Phys. Status Solidi A **32**, 631 (1975).

[11]H.-G. Brühl, L. Hildisch, H. Morwinski, W. Schmidt, and E. Schubert, Phys. Status Solidi A **39**, 133 (1977).

[12]Y. Kashihara, N. Kashiwagura, M. Sakata, J. Harada, and T. Arii, Jpn. J. Appl. Phys. **23**, L901 (1984).

[13]C. Bocchi, P. Franzosi, and C. Ghezzi, J. Appl. Phys. **57**, 4533 (1984).

[14]K. Osamura, M. Sugahara, and K. Nakajima, Jpn. J. Appl. Phys. **26**, L1746 (1987).

[15]S. Yasuami, K. Koga, K. Ohshima, S. Sasaki, and M. Ando, J. Appl. Crystallogr. **25**, 514 (1992).

[16]H. Okuda, M. Kondo, K. Kato, and K. Nakajima, Appl. Phys. Lett. **56**, 337 (1990).

[17]A. G. Norman and G. R. Booker, in *Microscopy of Semiconducting Materials 1985,* edited by A. G. Cullis and D. B. Holt, IOP Conf. Proc. No. 76 (Institute of Physics and Physical Society, London, 1985), Sec. 6, p. 257.

[18]J. P. Gowers, Appl. Phys. A **31**, 23 (1983).

[19]H. W. M. Salemink and O. Albrektsen, Phys. Rev. B **47**, 16 044 (1993).

[20]J. F. Zheng, J. D. Walker, M. B. Salmeron, and E. R. Weber, Phys. Rev. Lett. **72**, 2414 (1994).

[21]D. B. Zax, S. Vega, N. Yellin, and D. Zamir, Chem. Phys. Lett. B **8**, 105 (1987).
[22]R. Tycko, G. Dabbagh, S. R. Kurtz, and J. P. Goral, Phys. Rev. B **45**, 13 452 (1992).
[23]D. B. Zax, D. Zamir, and S. Vega, Phys. Rev. B **47**, 6304 (1993).
[24]A. Kobayashi and A. Roy, Phys. Rev. B **35**, 5611 (1987).
[25]I. Sela, V. V. Gridin, R. Beserman, R. Sarfaty, D. Fekete, and H. Morkoç, J. Appl. Phys. **63**, 966 (1988).
[26]I. Sela and R. Beserman, Phys. Rev. B **39**, 3254 (1989).
[27]R. Manor, O. Brafman, D. Fekete, and R. Sarfaty, Phys. Rev. B **47**, 9492 (1993).
[28]H. W. Verleur and A. S. Barker, Phys. Rev. **149**, 715 (1966).
[29]S. Yamazaki, A. Ushirokawa, and T. Katoda, J. Appl. Phys. **51**, 3722 (1980).
[30]S. Perkowitz, L. S. Kim, and P. Becla, Phys. Rev. B **43**, 6598 (1991).
[31]S. Lai and M. V. Klein, Phys. Rev. Lett. **44**, 1087 (1980).
[32]L. Samuelson, S. Nilsson, Z.-G. Wang, and H. G. Grimmeiss, Phys. Rev. Lett. **53**, 1501 (1984).
[33]E. F. Schubert, E. O. Göbel, Y. Horikoshi, K. Ploog, and H. J. Queisser, Phys. Rev. B **30**, 813 (1984).
[34]S. Shirakata, T. Nishino, and Y. Hamakawa, J. Appl. Phys. **63**, 484 (1988).
[35]A. Dimoulas, Z. Hatzopoulos, I. Stoemenos, and A. Christou, Superlatt. Microstruct. **8**, 117 (1990).
[36]R. C. Kittler and L. M. Falicov, J. Phys. C **10**, 1667 (1977).
[37]Y. Fu, K. A. Chao, and R. Osório, Phys. Rev. B **40**, 6417 (1989).
[38]R. Magri, S. Froyen, and A. Zunger, Phys. Rev. B **44**, 7947 (1991).
[39]K. A. Mäder and A. Zunger, Appl. Phys. Lett. **64**, 2882 (1994).
[40]ρ should not be confused with the density matrix of a thermodynamic ensemble. $\rho(\sigma)$ gives the weight of a configuration σ in a *configurational average* at zero temperature, rather than in an *ensemble average* at finite temperature.
[41]K. C. Hass, L. C. Davis, and A. Zunger, Phys. Rev. B **42**, 3757 (1990).
[42]Z. Q. Li and W. Pötz, Phys. Rev. B **46**, 2109 (1992).
[43]A. Silverman, A. Zunger, R. Kalish, and J. Adler, J. Phys. Condens. Matter (to be published).
[44]J. M. Sanchez, F. Ducastelle, and D. Gratias, Physica A **128**, 334 (1984).
[45]For a review, see A. Zunger, in *Statics and Dynamics of Alloy Phase Transformations,* Vol. 319 of *NATO Advanced Study Institute, Series B: Physics,* edited by P. E. A. Turchi and A. Gonis (Plenum, New York, 1994).
[46]A. Zunger, S.-H. Wei, L. G. Ferreira, and J. E. Bernard, Phys. Rev. Lett. **65**, 353 (1990).
[47]S.-H. Wei, L. G. Ferreira, J. E. Bernard, and A. Zunger, Phys. Rev. B **42**, 9622 (1990).
[48]Z.-W. Lu, S.-H. Wei, and A. Zunger, Phys. Rev. B **44**, 10 470 (1991); **44**, 3387 (1991); **45**, 10 314 (1992).
[49]L. G. Ferreira, S.-H. Wei, and A. Zunger, Int. J. Supercomput. Appl. **5**, 34 (1991).
[50]S. Kirkpatrick, C. D. Gelatt, and M. P. Vecchi, Science **220**, 671 (1983).
[51]N. Metropolis, A. Rosenbluth, M. Rosenbluth, A. Teller, and E. Teller, J. Chem. Phys. **21**, 1087 (1953).
[52]Detailed descriptions of the SQS's available in electronic archive ftp://ftp.nrel.gov/pub/sst/archive/sqs.
[53]P. N. Keating, Phys. Rev. **145**, 637 (1966); R. M. Martin, Phys. Rev. B **1**, 4005 (1970).
[54]We use in the VFF model of Ref. 53 the experimental equilibrium bond lengths when we compare the relaxed alloy geometry with experiment. When results are compared with alloy LDA results, we use in Keating's model LDA-calculated bond lengths.
[55]J. C. Mikkelsen and J. B. Boyce, Phys. Rev. Lett. **49**, 1412 (1982).
[56]R. Magri, S.-H. Wei, and A. Zunger, Phys. Rev. B **42**, 11 388 (1990); Z.-W. Lu, S.-H. Wei, A. Zunger, S. Frota-Pessoa, and L. G. Ferreira, *ibid.* **44**, 512 (1991).
[57]Multisite CPA calculations of the density of states have been performed for transition-metal alloys with SRO; however, they neglect atomic relaxation. See, for example, N. Takano, S. Imai, and M. Fukuchi, J. Phys. Soc. Jpn. **60**, 4218 (1991).
[58]A.-B. Chen and A. Sher, Phys. Rev. B **23**, 5360 (1981).
[59]K. A. Mäder and A. Zunger, Phys. Rev. B **50**, 17 393 (1994).
[60]L.-W. Wang and A. Zunger, J. Chem. Phys. **100**, 2394 (1994); J. Phys. Chem. **98**, 2158 (1994).
[61]M. Jaros, Rep. Prog. Phys. **48**, 1091 (1985).
[62]The spectral density of Eq. (11) is related to $A(\mathbf{k},E)$ of Ref. 41 by the trace over all bands, i.e., $A(\mathbf{k},E)=\sum_n A_n(\mathbf{k},E)$.
[63]W. Ge, W. D. Schmidt, M. D. Sturge, L. N. Pfeiffer, and K. W. West, J. Lumin. **59**, 163 (1994).
[64]H. J. Lee, L. Y. Juravel, J. C. Woolley, and A. J. SpringThorpe, Phys. Rev. B **21**, 659 (1980).
[65]H. Temkin and V. G. Keramidas, J. Appl. Phys. **51**, 3269 (1980).
[66]W. B. Wang, R. R. Alfano, D. Szmyd, and A. J. Nozik, Phys. Rev. B **46**, 15 828 (1992).
[67]A. K. Saxena, Phys. Status Solidi B **105**, 777 (1981).
[68]A.-B. Chen and A. Sher (private communication).
[69]G. Kerker, J. Phys. C **13**, L189 (1980).
[70]D. M. Ceperley and B. J. Alder, Phys. Rev. Lett. **45**, 566 (1980).
[71]J. P. Perdew and A. Zunger, Phys. Rev. B **23**, 5048 (1981).
[72]S. Froyen, Phys. Rev. B **39**, 3168 (1989).
[73]The Fourier quadrature **k** points are generated from a bcc grid of 256 reducible points in the fcc Brillouin zone, except for SQS-16, where a bcc grid of 64 reducible points is used.
[74]The shifts pertinent to the present alloys $Al_{0.5}Ga_{0.5}As$, $Ga_{0.5}In_{0.5}P$, and $Al_{0.5}In_{0.5}As$ are 0.84, 0.61, and 0.77 eV, respectively. This proceudre does not affect energy differences such as optical bowing coefficients.
[75]*Semiconductors. Physics of Group IV Elements and III-V Compounds,* edited by O. Madelung, M. Schulz, and H. Weiss, Landolt-Börnstein, New Series, Group III, Vol. 17, Pt. a (Springer, Berlin, 1982).
[76]B. Wakefield, M. A. G. Halliwell, T. Kerr, D. A. Andrews, G. J. Davies, and D. R. Wood, Appl. Phys. Lett. **44**, 341 (1984).
[77]T. Kurimoto and N. Hamada, Phys. Rev. B **40**, 3889 (1989).
[78]R. G. Alonso, A. Mascarenhas, G. S. Horner, K. A. Bertness, S. R. Kurtz, and J. M. Olson, Phys. Rev. B **48**, 11 833 (1993).
[79]A. Baldereschi and J. J. Hopfield, Phys. Rev. Lett. **28**, 171 (1972).
[80]H. P. Hjalmarson, P. Vogl, D. J. Wolford, and J. D. Dow, Phys. Rev. Lett. **44**, 810 (1980).
[81]We envision the substitutional $A_{1-x}B_x$ alloy on a fcc lattice as a "cluster alloy" composed of $A_{4-n}B_n$ tetrahedra placed on simple cubic lattice sites. A given degree of nearest-neighbor SRO in the alloy is then reflected by a change of concentration of the different clusters, e.g., increase of the number of A_4 and B_4 clusters with respect to the mixed ones for $\alpha>0$. Note that this simplification neglects the fact that in the real alloy, each atom participates in several inter-

penetrating clusters instead of just one.
[82]For a review, see I. M. Lifshitz, Usp. Fiz. Nauk **83**, 617 (1964) [Sov. Phys. Usp. **7**, 549 (1965)].
[83]S.-H. Wei and A. Zunger, Phys. Rev. Lett. **59**, 144 (1987).
[84]D. J. Wolford, in *Physics of Semiconductors: Proceedings of the 18th International Conference, Stockholm, 1986,* edited by O. Engström (World Scientific, Singapore, 1987), p. 1115.
[85]R. G. Dandrea (private communication).
[86]S.-H. Wei (private communication).